Scatterer and Virtual Source Detection for Indoor UWB Channels

Markus Froehle, Paul Meissner, Thomas Gigl and Klaus Witrisal
Graz University of Technology, Graz, Austria. Email: froehle@student.tugraz.at; {paul.meissner, thomas.gigl, witrisal}@tugraz.at

***Abstract*—We present an extension of an existing outdoor UWB scatterer detection algorithm [1], [2], making it usable for indoor scenarios. The algorithm is extended with the capability to find virtual sources, which can explain reflections from extended, plane surfaces. The extension thus removes the restriction to just single-bounce signal paths. Single-bounce scatterers, as well as virtual sources extracted from the channel impulse response, are assigned to positions in 2-dimensional space and can be matched to given floor plan information. The functionality is demonstrated with indoor measurement data obtained in a large office environment that represents a challenging dense multipath scenario. Results show that estimated locations of virtual sources and scatterers fit very well with the expected locations.**

I. Introduction

Ultra wide-band (UWB) signals are promising candidates as sensing signals in e.g. indoor localization applications, because of the large available frequency range of $3.1 - 10.6\,\text{GHz}$. This offers a fine delay resolution and robustness in harsh environments [3]. In [4], multipath propagation is described as a phenomenon where signals reach the receive antenna via multiple paths, arising from either reflections or scattering, leading to dependencies in the arrival times of the multipath components (MPCs). A distinguishing feature of the UWB indoor channel is that many of these individual paths are recognizable and resolvable in the measurements [5].

The work presented in this paper is motivated by a multipath-aided indoor localization approach. Localization based on range estimates can be done by multilateration of at least three known reference nodes. Such methods tend to be error-prone in non line-of-sight (NLOS) situations, leading to a bias in the position error. In [6] and [7] we have shown an approach to overcome the NLOS problem by incorporating a-priori known floor plan information and exploiting the MPCs, allowing localization with only one reference node. An implementation of such a system would need an algorithm for MPC extraction, that is ideally able to run on a low-complexity, single antenna device. In the literature, many approaches are found for multipath extraction algorithms, e.g. SAGE [8] or CLEAN [9]. Often, measurements performed with an array are used, which might not be practical in an actual indoor localization system. In [1] and [2], an algorithm extracting MPCs from channel impulse responses (CIRs) measured along a trajectory was proposed for analysis of outdoor measurement data.

This work was partly supported by the Austrian Science Fund (FWF) within the National Research Network SISE project S10604-N13.

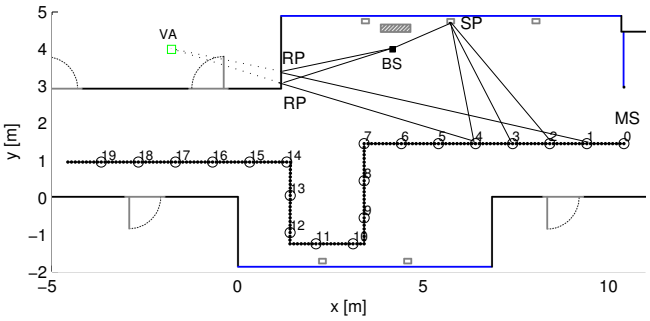

Fig. 1. Indoor measurement scenario showing receiver base station (BS) and trajectory of the 200 transmitter mobile station (MS) positions. Concrete walls are plotted in black, glass walls in blue and metal parts in grey. A large concrete pillar is located behind the BS. The relationship between BS, MS, reflection point (RP), scatterer point (SP) and virtual anchor (VA) is shown.

In this paper, we present an extension of this algorithm that accounts for reflections at extended plane surfaces in an indoor scenario. Instead of estimating scatterer positions only, we also estimate the positions of virtual sources, so-called virtual anchors (VAs). VAs can also account for higher-order reflections and are potentially useful for localization [7]. We demonstrate the suitability of the extension with recently obtained measurement data from an indoor environment.

The remainder of this paper is structured as follows: Section II describes the indoor measurement scenario, Section III gives an overview of the algorithm in [1] and [2] and describes our extension to it. Finally, Section IV discusses the results we have obtained.

II. Indoor Scenario, Measurements and Geometry

A. Measurement Scenario

The channel measurements have been performed in an indoor scenario, i.e. a hallway at our department at Graz University of Technology. The floor plan, including receiver (here the base station (BS)) and transmitter (the mobile station (MS)) positions, is illustrated in Fig. 1. Floor, walls and part of the ceiling are made of concrete, doors and some smaller pillars are made of metal. The hallway has two large glass fronts reaching from floor to ceiling, shown in blue in the floor plan. The height of the open ceiling is varying, due to smaller hallways at the sides of the two upper floors, which are connected by bridges made of metal and concrete. The MS is moved along a trajectory containing 200 positions with a spacing of $10\,\text{cm}$, as illustrated in Fig. 1. For all

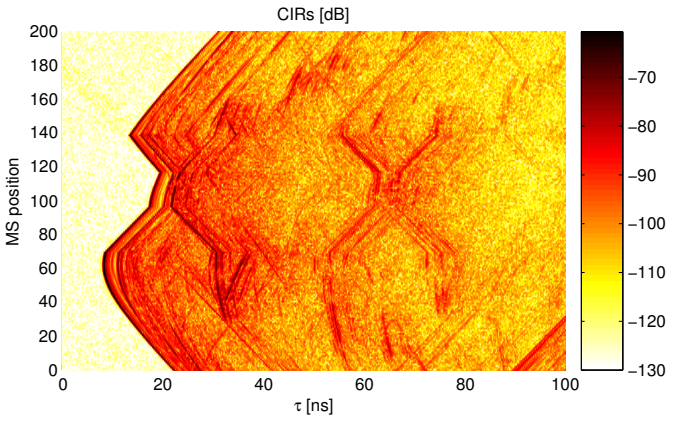

Fig. 2. Measured channel impulse responses (CIRs) over the trajectory of MS positions. A multitude of strong multipath components is clearly visible behind the strong LOS path. Only a part of the delay axis is shown.

MS positions, the complex channel transfer function between transmitter MS and receiver BS was measured using a Rhode & Schwarz ZVA-24 vector network analyzer. Table I contains the measurement parameters. Fig. 2 shows the measured CIRs over the trajectory of MS positions.

TABLE I
MEASUREMENT SETUP

Parameter	Value
Scenario	Indoor hallway with concrete walls, large glass fronts and metal pillars
No. of MS positions	200, spacing 10 cm
Frequency range	$6-8$ GHz
Frequency spacing	1 MHz
Network Analyzer	Rhode & Schwarz ZVA-24
Antennas	Skycross SMT-3TO10M plus custom made 5-cent coin antenna
Antenna height	1.5 m

B. Scatterer Points and Virtual Anchors

We define a scatterer point (SP) as the point in space where a wave travelling from transmitter to receiver seems to origin from, e.g. a small pillar. For reflections at plane surfaces, we also define reflection points (RPs) as SPs that follow multipath geometry [4], i.e. that will move as the TX and/or RX moves. Incorporating the floor plan, a wave that is subject to this surface reflection can be associated to a virtual source. Due to our use of these points for localization [6], we call them virtual anchors (VAs). VAs are mirror images of the anchor with respect to the room walls, or other reflecting surfaces [5]. Fig. 1 illustrates examples and the relation between SP, RP and VA.

III. MULTIPATH DETECTION ALGORITHM

A. System Model

To model the UWB channel, we use the well-known model of the impulse response described by the summation of closely-spaced, scaled impulses [3]

$$x(\tau) = \sum_{k=1}^{L} \alpha_k \delta(\tau - \tau_k). \tag{1}$$

Here, L is the number of MPCs, α_k the corresponding scaling factor and $\delta(\tau)$ the Dirac-delta impulse. If the k-th MPC corresponds to a single-scattering process, the delay τ_k can be described in the spatial domain by the sum of the path-lengths between MS-SP and SP-BS. Neglecting any dielectric media the wave travels with speed of light $c \approx 3 \cdot 10^8 m/s$, corresponding to a delay

$$\tau_{k_{\mathrm{SP}}} = \frac{d(\mathrm{MS},\mathrm{SP}) + d(\mathrm{SP},\mathrm{BS})}{c}. \tag{2}$$

Here, $d(\mathrm{MS},\mathrm{SP})$ is the geometric distance between the two points MS and SP and $d(SP,BS)$ the distance between SP and BS, respectively.

If the k-th MPC is caused by e.g. a reflection at a room wall, the VA model can be used and the delay is

$$\tau_{k_{\mathrm{VA}}} = \frac{d(\mathrm{VA},\mathrm{MS})}{c} \tag{3}$$

where $d(\mathrm{VA},\mathrm{MS})$ corresponds to the geometric distance between VA and MS. The VA model aids in geometric calculations. Virtual sources could be replaced by virtual sinks as seen from the transmitter MS [5].

Note, that the concept of VAs takes higher-order specular reflections into account implicitly. The delay of a VA representing a single or multiple reflections is simply described by the location of the corresponding VA. We will show how our algorithm is able to locate VAs responsible for e.g. double reflections.

B. Algorithm for Multipath Extraction and Scatterer Detection

We implemented the algorithm in [1] and [2], which was originally intended for an outdoor scenario. For the sake of completeness the algorithm is shortly reviewed here, followed by a description of our extension to make it suitable for an indoor scenario. Based on the frequency domain measurements, the algorithm detects scatterer points in three computation steps

- Step I - High resolution peak search in time domain
- Step II - Spatial weighting of all candidate scatterers
- Step III - Detection/cancellation of strongest scatterer.

In step I, the measured complex channel transfer functions for all MS positions are transformed into time domain using a certain amount of oversampling. In the CIRs, all peaks above a threshold μ are then estimated using a *search and subtract* approach. The subtraction of a peak in the CIR itself is performed in frequency domain. In step II, a geometric 2-dimensional grid search is done over the l-th grid position for scatterer identification by a comparison of the candidate scatterer delay $\tau_{l_{\mathrm{SP}}}$ with the delays of all the estimated peaks. If they are within one delay resolution τ_{res}, their amplitude is stored as a function of the MS position index. The parameter τ_{res} is defined as the inverse of the measurement bandwidth.

Next, an average sliding window with window length N_W is applied to the amplitudes over all MS positions. Using the same threshold value μ as in step I, a scatterer's *birth* is defined when the averaged amplitude exceeds the threshold. Its *death* is reached, when the amplitude drops below μ. The *strength* $s_{l,\mathrm{SP}}$ of the l-th candidate scatterer is computed by the summation of all peak amplitudes during its lifetime. In step III, the candidate scatterer with the highest strength is estimated according to

$$l_{\mathrm{SP,max}} = \underset{l}{\mathrm{argmax}}(s_{l,\mathrm{SP}}) \tag{4}$$

and then deleted from the channel, following the same *search and subtract* approach as in step I. The steps are repeated until all or a defined number of scatterers have been identified.

C. Extension for Estimating VAs

We extended step II to also account for VAs: Not only $\tau_{l_{\mathrm{SP}}}$, but also $\tau_{l_{\mathrm{VA}}}$ is used as hypothesis for each grid position. The point with the largest strength will then be chosen as

$$l_{\max} = \underset{l}{\mathrm{argmax}}(s_{l_{\mathrm{SP,max}}}, s_{l_{\mathrm{VA,max}}}). \tag{5}$$

Here, $l_{\max}$ is the index of the grid position that corresponds to the maximum of the strongest scatterer $s_{l_{\mathrm{SP,max}}}$ and the strongest VA $s_{l_{\mathrm{VA,max}}}$ over all grid positions. The advantage of this method is that, due to the same weight estimation, always the more likely one will be detected and removed from the channel. In comparison to the outdoor scenario in [1], we expect the higher density of MPCs in an indoor scenario to cause problems. Especially in the application of the average sliding window, this and the diffuse scattered components can cause the detection threshold to be exceeded, although the respective candidate scatterer is not responsible for this.

IV. Performance Results

A. Choice of Parameters

The frequency range is reaching from 6 to 8GHz, which results in a spatial resolution of

$$d_{\mathrm{spatial}} = c \cdot \tau_{\mathrm{res}} = c \cdot \frac{1}{f_{\max} - f_{\min}} \approx 15\,\mathrm{cm} \tag{6}$$

where τ_{res} is the delay resolution. $f_{\max}$ and $f_{\min}$ are the maximum and minimum frequency and c is the speed of light. In contrast to this, using a bandwidth from 3.1 to 10.6GHz results in a spatial resolution of $d_{\mathrm{spatial}} \approx 4$cm.

The time delay resolution $\Delta\tau$ of the high resolution peak search in step I is set four times smaller than the delay resolution, $\Delta\tau = \tau_{\mathrm{res}}/4$. The spatial search step d_{res} of the grid search in step II is set two times smaller than the systems spatial resolution, i.e. $d_{\mathrm{res}} = d_{\mathrm{spatial}}/2 \approx 7.5\,\mathrm{cm}$.

B. Results: Estimated Scatterer and VA Locations

Fig. 3 contains the first 16 estimated VA and SP positions plotted in 2-dimensional spatial domain. Expected VA locations are marked by a green square. Most of them have been identified by the algorithm. Expected VAs, which are only visible for a few MS positions, could not be identified. This is because the number of CIRs, which contain a peak caused by the VA, are low. Therefore, the strength of a candidate VA is lower than others and not selected by the algorithm.

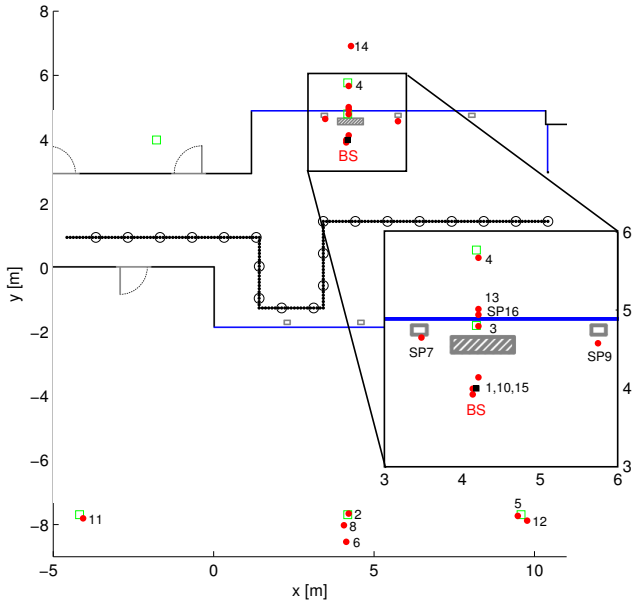

Fig. 3. Estimated VAs and SPs together with the floor plan. VAs and SPs are plotted as red dots and labelled with the iteration number in which they were estimated. Green squares indicate expected VAs. BS, the metal pillars beside the BS and most of the strongest VAs have been found by the algorithm.

The two expected VAs at position $[-4.2, -7.7]^{\mathrm{T}}$ and $[9.6, -7.7]^{\mathrm{T}}$ correspond to VAs of order two, i.e., double reflections between MS and BS. As can be seen in Fig. 3, the algorithm has identified also these higher-order VAs.

Certain VA/SP are identified more than once. Due to the used channel model and the choice of parameters it is not always possible to cancel the whole MPC from the channel at once. More iteration steps are needed, but the estimated positions of the VA or SP are closely spaced in the spatial domain. The two metal pillars close to the BS are detected as SPs 7 and 9. VA/SP numbering agrees with the iteration in which they have been estimated, i.e. it relates to the strength of the individual MPCs.

For the sake of completeness, we also report that at a higher bandwidth ($3.1 - 10.6\,\mathrm{GHz}$), the results did not deviate much from those presented here, although the estimates of the VA/SP locations were a little more exact. To evaluate its usefulness for MPC extraction, we mostly evaluated the limited bandwidth. In the following, we present an analysis of the algorithm steps, pointing out the peculiarities when using it in an indoor, dense-multi-path scenario. For this, we choose VA 2 and SP 9.

C. Step I - High Resolution Peak Search in Time Domain

This computation step estimates the exact delay of all peaks above the threshold μ in the CIRs of all MS positions. Fig.

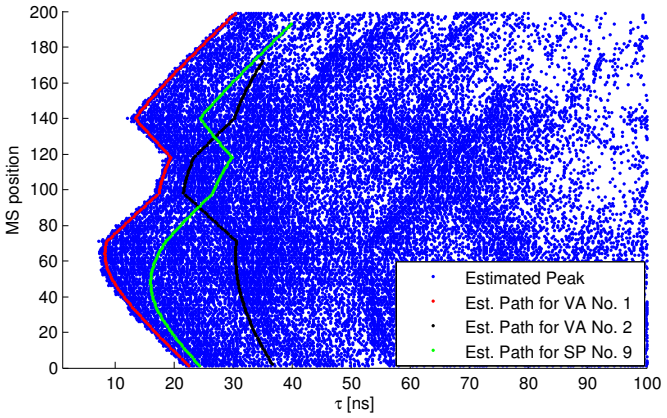

Fig. 4. All detected peaks above the threshold with their exact delays over the trajectory are plotted. Red, green and black correspond to the path of peaks selected for scatterer with number 1, 2 and 9, respectively.

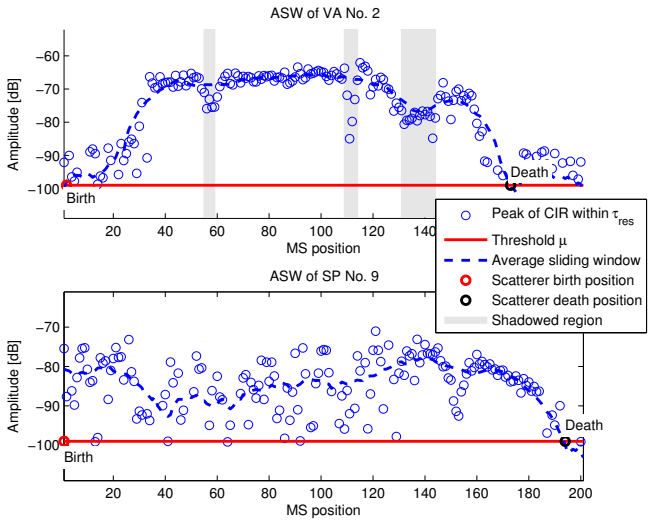

Fig. 5. Average sliding window (ASW) and peak amplitudes above threshold μ, which lie within one delay resolution τ_{res} of the delay of the VA. Upper plot: ASW of VA 2, lower plot: ASW of SP 9.

4 shows all the estimated peaks in iteration 1. The threshold μ was set to -99dB. There are no peaks estimated before the LOS. The indoor measurement scenario causes a lot of MPCs and results in a rather dense plot, but still, paths of accumulated peaks along the MS trajectory are visible. Depending on the measurements and the choice of parameter μ, the number of detected peaks in step I varies. Step II of the algorithm uses all detected peaks in order to find the strongest scatterer. If the threshold value μ is set too high, only a few, but strong, scatterer points are found. On the other hand, if μ is too close to the noise floor of the CIR, very many peaks are detected, but they might deteriorate the outcome resulting in a wrong scatterer detection and deletion from the channel. In the figure, the red path corresponds to VA 1 found in iteration one, which clearly matches the LOS path. The black and green path correspond to VA 2 and SP 9, respectively.

D. Step II - Spatial Weighting of All Candidate Scatterers

The upper plot of Fig. 5 shows the outcome of the average sliding window of VA 2 over all the estimated peaks which are within one delay resolution τ_{res}. Along the trajectory, one can see the significant increase of the amplitudes as soon as the VA becomes visible (compare with Fig. 1). Also the amplitude value does not change rapidly between neighboring MS positions. A drop of the amplitude is noticeable between MS position 55 and 59, because the signal path is blocked by a metal pillar between the MS and VA. Another pillar blocks the VA approximately between MS position 109 and 114 and again between 131 and 144.

The sliding window averages the amplitude of the single peaks along the trajectory and defines the scatterer's lifetime. The algorithm has estimated the birth of the VA at MS position 1 and its death at position 173. According to the floor-plan, the VA is visible, in contrast to this, between position 30 and 160, neglecting the MS positions where the pillars cover the view to the VA. The lifetime is severely overestimated, because there are some peaks outside the visibility region. The delays of these peaks lie within τ_{res}, but they might correspond to other scatterers — reflecting the high density of scatterer in our indoor scenario —, or to diffuse multipath components.

The estimated lifetime of SP 9, shown in the lower plot, takes this to an extreme. There are many peaks estimated within τ_{res} with the delay corresponding to the path-length of the scatterer. Up to MS position 140, the amplitudes of neighboring MS positions are strongly fluctuating, suggesting they are caused by other scatterers having the same delay. Starting from MS 140 to 180 there is a stronger correlation in the amplitudes of neighboring MS positions. The amplitude loss at MS 150 might be caused by the geometry of the pillar itself. The life-time of the SP can be said to lie roughly between MS 140 and 180, but the algorithm estimated it between MS 1 and 194. The high number of peaks between the scatterers birth and death and the long lifetime leads to the strongest weight over all candidate scatterers for this iteration. We identify the exploitation of the different amplitude characteristics in blocked and visible positions as potential for future work.

Fig. 6 depicts the VA strength s_l for two successive iterations in 2-dimensional space overlaid by the floor-plan. The left column shows the entire search space; the right column provides close-up views at the positions of the highest VA strengths. The peaks in the CIRs corresponding to these VAs will be removed from the channel. In the next iteration, the VA is removed and therefore the strength at this point decreased.

In order to estimate a scatterer position in spatial domain, the algorithm compares its delay τ with the delay of the peaks exceeding the threshold μ in all CIRs. This can lead to ambiguous scatterer points in space if the MS trajectory is a straight line. For example, in the upper left plot of Fig. 6 there is a point with high strength exactly at the horizontally down-flipped position of the BS at coordinates $[4.2, -1.0]^{\mathrm{T}}$. Once the scatterer at the BS is removed from the channel,

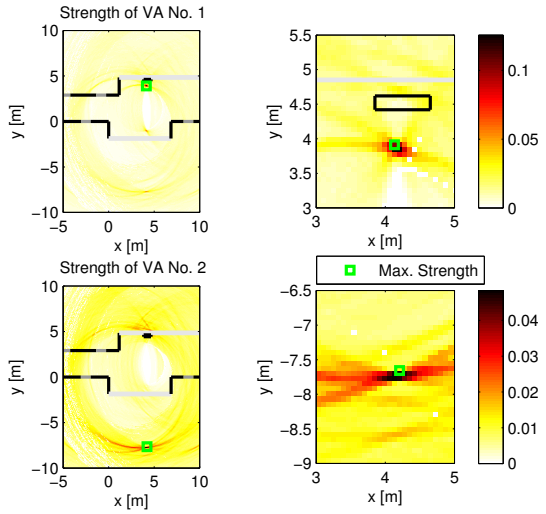

Fig. 6. VA strength plotted in 2-dimensional spatial domain. The strength is encoded in color. Left: Strength in entire search space. Right: Close-up view at the location of the estimated VA from the left hand-side. Upper row: Strength of VA 1. Lower row: Strength of VA 2.

the ambiguous scatterer is also removed. This can be seen in the lower left plot, where the ambiguous scatterer disappeared completely. In the presented scenario, this ambiguity was resolved since the trajectory consists of straight segments as well as 90° curves.

E. Step III - Detection and Cancellation of the Strongest Scatterer

Fig. 7 shows the original, measured CIRs over the trajectory and illustrates the effect of the successive scatterer deletion. The LOS component clearly has the strongest amplitude and the lowest delay τ between MS and BS. The artefacts with a shorter delay than the LOS are due to the rectangular windowing caused by the bandwidth limitation to $6-8$ GHz. The LOS scatterer is the first one to be selected and removed from the channel by the algorithm. The lower plot contains the CIRs after 16 iterations. The paths of peaks associated with the first 16 scatterer positions are now removed from the channel.

V. Conclusions and Future Work

We have presented an extension to an algorithm for outdoor UWB scatterer detection [1], making it usable in indoor environments. The extension to estimate virtual sources in addition to single-bounce scatterers, allows us to apply the algorithm to scenarios with a high density of diffuse MPCs. Also, we were able to resolve higher-order reflections with the concept of VAs. We demonstrated the functionality of our extension with indoor UWB measurement data. Results show that the localization of VAs in 2-dimensional spatial domain works very well. Problems are seen in the application of the sliding window to estimate the lifetime of an SP/VA for our indoor scenario due to the high density of MPCs. Further improvements of the algorithm should focus on this and the reduction of computational effort for the high resolution peak search in step I and the grid search in step II.

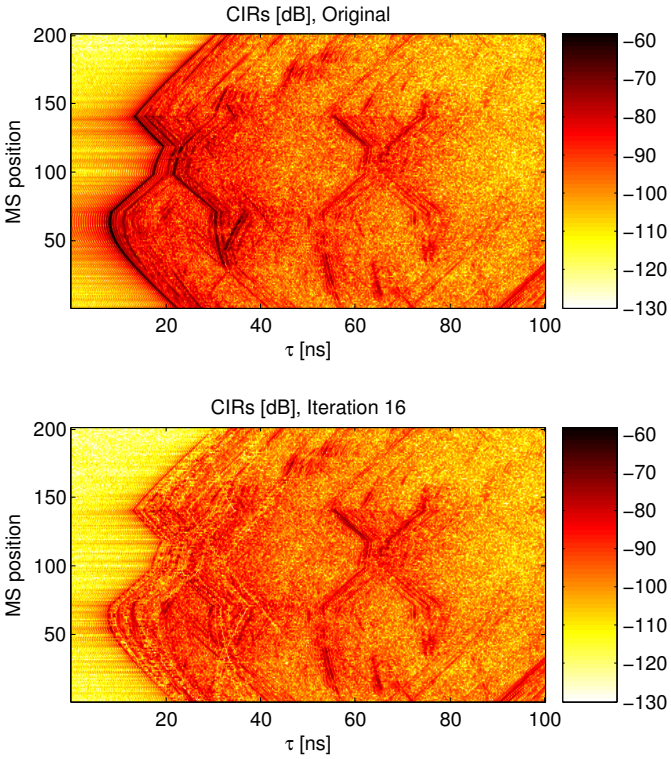

Fig. 7. Upper plot: Measured CIRs over trajectory, the left-most strongest path with a high amplitude along the trajectory corresponds to the LOS path. The artefacts with a shorter delay than the LOS are caused by the rectangular windowing due to the bandwidth limitation to $6-8$ GHz. Lower plot: CIRs after removing the first 16 VAs/SPs. The path of peaks associated with them have been removed.

References

[1] T. Santos, J. Karedal, P. Almers, F. Tufvesson, and A. Molisch, "Scatterer Detection by Successive Cancellation for UWB - Method and Experimental Verification," in *Vehicular Technology Conference, 2008. VTC Spring 2008. IEEE*, May 2008, pp. 445 –449.

[2] ——, "Modeling the ultra-wideband outdoor channel: Measurements and parameter extraction method," *Wireless Communications, IEEE Transactions on*, vol. 9, no. 1, pp. 282 –290, 2010.

[3] A. Molisch, "Ultra-Wide-Band Propagation Channels," *Proceedings of the IEEE*, vol. 97, no. 2, pp. 353 –371, 2009.

[4] Y. Shen and M. Win, "On the use of multipath geometry for wideband cooperative localization," in *Global Telecommunications Conference, 2009. GLOBECOM 2009. IEEE*, 302009-dec.4 2009, pp. 1 –6.

[5] J. Kunisch and J. Pamp, "An ultra-wideband space-variant multipath indoor radio channel model," in *Ultra Wideband Systems and Technologies, 2003 IEEE Conference on*, 16-19 2003, pp. 290 – 294.

[6] P. Meissner, C. Steiner, and K. Witrisal, "UWB positioning with virtual anchors and floor plan information," in *Positioning Navigation and Communication (WPNC), 2010 7th Workshop on*, 2010, pp. 150 –156.

[7] P. Meissner, T. Gigl, and K. Witrisal, "UWB sequential Monte Carlo positioning using virtual anchors," in *Indoor Positioning and Indoor Navigation (IPIN), 2010 International Conference on*, 2010, pp. 1 –10.

[8] B. Fleury, M. Tschudin, R. Heddergott, D. Dahlhaus, and K. Ingeman Pedersen, "Channel parameter estimation in mobile radio environments using the sage algorithm," *Selected Areas in Communications, IEEE Journal on*, vol. 17, no. 3, pp. 434 –450, Mar. 1999.

[9] R.-M. Cramer, R. Scholtz, and M. Win, "Evaluation of an ultra-wide-band propagation channel," *Antennas and Propagation, IEEE Transactions on*, vol. 50, no. 5, pp. 561 –570, May 2002.